Robust destriping method with unidirectional total variation and framelet regularization

Yi Chang,[1] Houzhang Fang,[1] Luxin Yan,[*] and Hai Liu

Key Laboratory of Ministry of Education for Image Processing and Intelligent Control, School of Automation, Huazhong University of Science and Technology, Wuhan, Hubei 430074, China

[1]*These authors contributed equally to this work.*

[*]*yanluxin@gmail.com*

Abstract: Multidetector imaging systems often suffer from the problem of stripe noise and random noise, which greatly degrade the imaging quality. In this paper, we propose a variational destriping method that combines unidirectional total variation and framelet regularization. Total-variation-based regularizations are considered effective in removing different kinds of stripe noise, and framelet regularization can efficiently preserve the detail information. In essence, these two regularizations are complementary to each other. Moreover, the proposed method can also efficiently suppress random noise. The split Bregman iteration method is employed to solve the resulting minimization problem. Comparative results demonstrate that the proposed method significantly outperforms state-of-the-art destriping methods on both qualitative and quantitative assessments.

©2013 Optical Society of America

OCIS codes: (100.0100) Image processing; (100.3020) Image reconstruction-restoration.

References and links

1. S.-W. Chen and J. L. Pellequer, "DeStripe: frequency-based algorithm for removing stripe noises from AFM images," BMC Struct. Biol. **11**(1), 7–16 (2011).
2. A. H. Lettington, S. Tzimopoulou, and M. P. Rollason, "Nonuniformity correction and restoration of passive millimeter-wave images," Opt. Eng. **40**(2), 268–274 (2001).
3. A. R. Harvey and R. Appleby, "Passive mm-wave imaging from UAVs using aperture synthesis," J. Aeronautical **107**, 87–98 (2003).
4. P. Rakwatin, W. Takeuchi, and Y. Yasuoka, "Stripe noise reduction in MODIS data by combining histogram matching with facet filter," IEEE Trans. Geosci. Rem. Sens. **45**(6), 1844–1856 (2007).
5. J. Torres and S. O. Infante, "Wavelet analysis for the elimination of striping noise in satellite images," Opt. Eng. **40**(7), 1309–1314 (2001).
6. J. J. Pan and C. I. Chang, "Destriping of Landsat MSS images by filtering techniques," Photogramm. Eng. Remote Sensing **58**, 1417–1423 (1992).
7. B. Münch, P. Trtik, F. Marone, and M. Stampanoni, "Stripe and ring artifact removal with combined wavelet--Fourier filtering," Opt. Express **17**(10), 8567–8591 (2009).
8. P. Mather, *Computer Processing of Remotely-Sensed Images: An Introduction* (Wiley, 2004).
9. R. Srinivasan, M. Cannon, and J. White, "Landsat data destriping using power filtering," Opt. Eng. **27**, 939–943 (1988).
10. J. S. Chen, Y. Shao, H. D. Guo, W. M. Wang, and B. Q. Zhu, "Destriping CMODIS data by power filtering," IEEE Trans. Geosci. Rem. Sens. **41**(9), 2119–2124 (2003).
11. F. L. Gadallah, F. Csillag, and E. J. M. Smith, "Destriping multisensor imagery with moment matching," Int. J. Remote Sens. **21**(12), 2505–2511 (2000).
12. H. F. Shen and L. P. Zhang, "A MAP-based algorithm for destriping and inpainting of remotely sensed images," IEEE Trans. Geosci. Rem. Sens. **47**(5), 1492–1502 (2009).
13. H. Carfantan and J. Idier, "Statistical linear destriping of satellite-based pushbroom-type images," IEEE Trans. Geosci. Rem. Sens. **48**(4), 1860–1871 (2010).
14. J. Fehrenbach, P. Weiss, and C. Lorenzo, "Variational algorithms to remove stationary noise: applications to microscopy imaging," IEEE Trans. Image Process. **21**(10), 4420–4430 (2012).
15. M. Bouali and S. Ladjal, "Toward optimal destriping of MODIS data using a unidirectional variational model," IEEE Trans. Geosci. Rem. Sens. **49**(8), 2924–2935 (2011).
16. N. Acito, M. Diani, and G. Corsini, "Subspace-based striping noise reduction in hyperspectral images," IEEE Trans. Geosci. Rem. Sens. **49**(4), 1325–1342 (2011).
17. X. Q. Liu, Y. L. Wang, and Y. Yuan, "Grahp-regularized low-rank representation for destriping of hyperspectral imges," IEEE Trans. Geosci. Rem. Sens. **51**(7), 4009–4018 (2013).

#196612 - $15.00 USD Received 28 Aug 2013; revised 11 Sep 2013; accepted 11 Sep 2013; published 24 Sep 2013

18. B. Datt, T. R. McVicar, T. G. Van Niel, D. L. B. Jupp, and J. S. Pearlman, "Preprocessing EO-1 Hyperion hyperspectral data to support the application of agricultural indexes," IEEE Trans. Geosci. Rem. Sens. **41**(6), 1246–1259 (2003).
19. X. X. Xiong, J. Q. Sun, W. Barnes, and V. Salomonson, "Multiyear on-orbit calibration and performance of Terra MODIS reflective solar bands," IEEE Trans. Geosci. Rem. Sens. **45**, 879–889 (2007).
20. L. X. Yan, H. Z. Fang, and S. Zhong, "Blind image deconvolution with spatially adaptive total variation regularization," Opt. Lett. **37**(14), 2778–2780 (2012).
21. H. Gao and H. K. Zhao, "Multilevel bioluminescence tomography based on radiative transfer equation Part 2: total variation and l1 data fidelity," Opt. Express **18**(3), 2894–2912 (2010).
22. E. Vera, P. Meza, and S. Torres, "Total variation approach for adaptive nonuniformity correction in focal-plane arrays," Opt. Lett. **36**(2), 172–174 (2011).
23. M. Freiberger, C. Clason, and H. Scharfetter, "Total variation regularization for nonlinear fluorescence tomography with an augmented Lagrangian splitting approach," Appl. Opt. **49**(19), 3741–3747 (2010).
24. J. F. Cai, R. H. Chan, and Z. W. Shen, "A framelet-based image inpaiting algorithm," Appl. Comput. Harmon. Anal. **24**(2), 131–149 (2008).
25. J. F. Cai, B. Dong, S. Osher, and Z. W. Shen, "Image restoration: total variation; wavelet frames; and beyond," J. Am. Math. Soc. **25**(4), 1033–1089 (2012).
26. J. F. Cai, H. Ji, C. Liu, and Z. W. Shen, "Framelet-based blind motion deblurring from a single image," IEEE Trans. Image Process. **21**(2), 562–572 (2012).
27. J. F. Cai, Framelet toolbox version 2.02, http://www.math.uiowa.edu/ jiancai/code/SplitBreg_Deblur.zip.
28. T. Goldstein and S. Osher, "The split bregman method for L1 regularized problems," SIAM J. Imag. Sci. **2**(2), 323–343 (2009).
29. D. L. Donoho, "De-noising by soft-thresholding," IEEE Trans. Inf. Theory **41**(3), 613–627 (1995).
30. X. Zhu and P. Milanfar, "Automatic parameter selection for denoising algorithms using a no-reference measure of image content," IEEE Trans. Image Process. **19**(12), 3116–3132 (2010).
31. D. L. Donoho and I. M. Johnstone, "Ideal spatial adaptation by wavelet shrinkage," Biometrika **81**(3), 425–455 (1994).
32. L. Holzer, F. Indutnyi, P. H. Gasser, B. Münch, and M. Wegmann, "Three-dimensional analysis of porous BaTiO3 ceramics using FIB nanotomography," J. Microsc. **216**(1), 84–95 (2004).
33. L. Holzer, P. H. Gasser, A. Kaech, M. Wegmann, A. Zingg, R. Wepf, and B. Muench, "Cryo-FIB-nanotomography for quantitative analysis of particle structures in cement suspensions," J. Microsc. **227**(3), 216–228 (2007).
34. A. Zingg, L. Holzer, A. Kaech, F. Winnefeld, J. Pakusch, S. Becker, and L. Gauckler, "The microstructure of dispersed and non-dispersed fresh cement pastes-new in-sight by cryo-microscopy," Cement Concr. Res. **38**(4), 522–529 (2008).
35. H. Liao and M. K. Ng, "Blind deconvolution using generalized cross-validation approach to regularization parameter estimation," IEEE Trans. Image Process. **20**(3), 670–680 (2011).

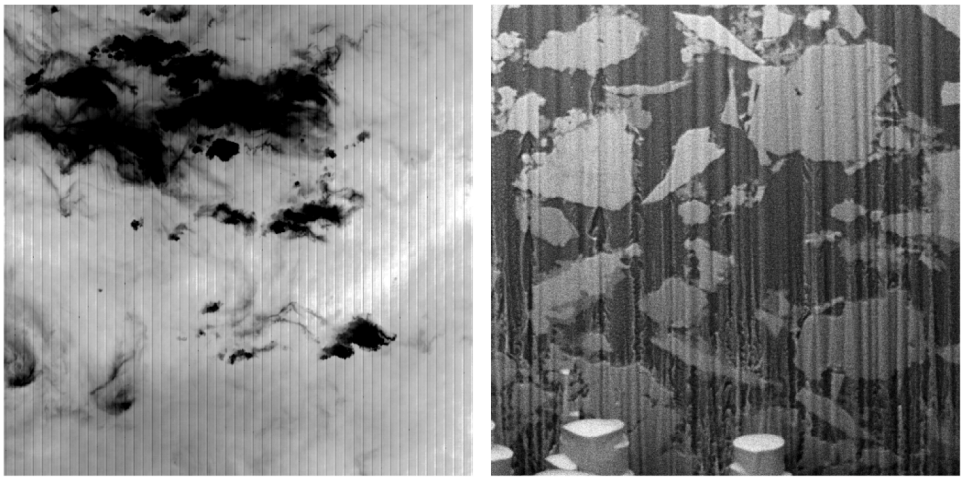
1. Introduction

Stripe noise commonly exists in multidetector imaging systems including the atomic force microscope (AFM) [1], passive millimeter-wave (PMMW) radio [2, 3], moderate resolution imaging spectroradiometer (MODIS) [4], and other such systems [5–7]. The main cause of stripe noise is the difference in the response of detectors, which severely limits the application of the resulting images. Therefore, it is critical to remove the stripes before the succeeding image interpretation processes are performed.

Many destriping methods have been proposed [1–11]. The first kind of destriping approach employs digital filtering in the transform domain [7–10] and suppresses the specific frequency caused by stripes. However, structural information with the same frequency will also be removed along with the stripes, thereby leading to image blurring and artifacts. The second kind of destriping approach, which includes methods such as histogram matching and moment matching [4, 11], focuses on the statistical property of digital numbers (DN) for each detector. To remove the stripes, the distribution of stripes is rectified to a reference one. These matching-based methods are highly limited by the similarity assumption [4].

The third kind of destriping approach treats the destriping issue as an inverse problem. An energy functional is constructed by imposing regularized constraints, and subsequently, it is minimized to obtain destriping results [12–17]. The stripe is often modeled as an additive process [14–17] or as both multiplicative and additive process [12]. In most imaging systems,

#196612 - $15.00 USD Received 28 Aug 2013; revised 11 Sep 2013; accepted 11 Sep 2013; published 24 Sep 2013
(C) 2013 OSA



(a) (b)

Fig. 1. (a) Regular stripes in moderate resolution imaging spectroradiometer (MODIS) image. (b) Irregular stripes in focused ion beam nanotomography (FIB-nt).

the degradation process contains both multiplicative and additive components, such as in the PMMW imaging system, and the push-broom imaging system [13]. In general, the stripes caused by the multiplicative component can be well calibrated [18, 19]. In this paper, the degradation process is described as

$$\mathbf{I}_s = \mathbf{u} + \mathbf{n}, \tag{1}$$

where $\mathbf{I}_s$ represents the striped image, and $\mathbf{u}$ is the latent unstriped image. The stripe noise $\mathbf{n}$ includes regular stripes [Fig. 1(a)] with strictly horizontal or vertical direction characteristics and irregular stripes [Fig. 1(b)] (for e.g., a stripe that is not perfectly straight, or with an offset value that is not constant over the whole length).

Stripe noise severely degrades the image quality, particularly the edge and detail information. The removal of stripe noise and preservation of edge and detail information is a very important and challenging problem. Total variation (TV) regularization is widely used due to its desirable properties such as convexity and the ability to preserve sharp edges [20–23]. Shen [12] firstly proposed a maximum-a-*posteriori* destriping method with a Huber–Markov prior, which means that the prior term is an alternative between TV regularization and Tikhonov regularization. A similar prior was also utilized in [14]. In [15], the authors proposed a sophisticated unidirectional TV model to remove regular stripes, in which it is assumed that the gradients along the stripes are not affected by the stripes. TV regularization is considered effective in removing the stripes but it cannot satisfactorily preserve structural details, thereby leading to structural information loss and piecewise constant effects.

Recently, framelet regularization has been employed in image restoration problems [24–26], where it is assumed that natural images have sparse representation under the framelet transform. The framelet has the ability of multiresolution analysis in nature, and therefore, it can adaptively capture multiscale edge structures in images. As a result, various types of edges can be well-preserved by framelet regularization. In this study, we propose a joint unidirectional TV and framelet regularization method to address the destriping problem. Our method utilizes the sparsity of the images in both the gradient and framelet domains. To the best of our knowledge, our method is the first one that introduces framelet regularization to address destriping. The main ideas and contributions of the proposed approach are summarized as follows:

#196612 - $15.00 USD Received 28 Aug 2013; revised 11 Sep 2013; accepted 11 Sep 2013; published 24 Sep 2013
(C) 2013 OSA

i) Unidirectional TV and framelet regularization are combined to address the destriping issue. The proposed method can effectively remove regular stripe noise with unidirectional TV regularization and preserve detail information via framelet regularization.

ii) The proposed method works well not only on regular stripes, but it also has the ability to remove irregular stripes from different kinds of images. Moreover, it can suppress random noise as well.

iii) The split Bregman algorithm is introduced to optimize the proposed model. The resulting optimization problem is split into several subproblems, which are very easy to implement.

The remainder of this paper is organized as follows. In section 2, we formulate the proposed model and the optimization algorithm. The experimental results and discussions are presented in section 3. Section 4 presents our conclusions.

2. Formulation and algorithm

2.1 Problem formulation

In this work, image destriping is formulated as an inverse problem by optimizing an energy functional including the data fidelity term and regularization term as follows:

$$\min_{\mathbf{u}} \Phi(\mathbf{u}-\mathbf{I}_s)+\lambda \mathrm{R}(\mathbf{u}), \tag{2}$$

where $\Phi(\mathbf{u}-\mathbf{I}_s)$ denotes the fidelity term, $\mathrm{R}(\mathbf{u})$ denotes the regularization term for a clear image, and λ denotes the regularization parameter.

We use the ℓ_2-norm as the fidelity term and design the regularization term $\mathrm{R}(\mathbf{u})$ to remove the stripe noise as well as preserve the edges and detail information:

$$\mathrm{R}(\mathbf{u})=\mathrm{R}_{\mathrm{TV}}(\mathbf{u})+\omega \mathrm{R}_{\mathrm{FR}}(\mathbf{u}). \tag{3}$$

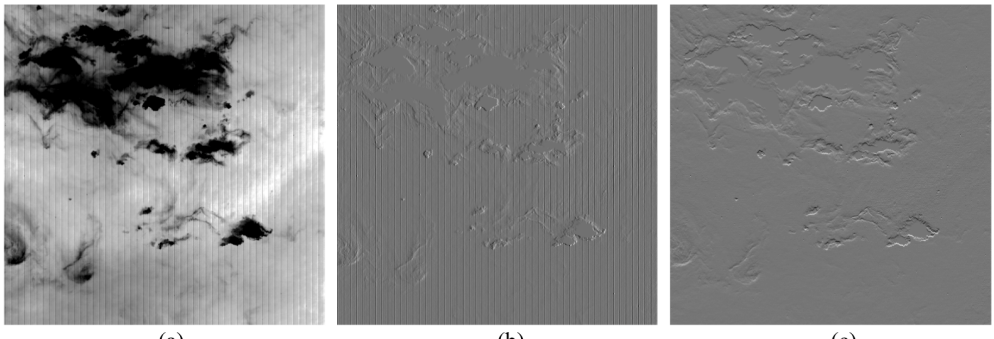
We argue that the isotropic TV is inappropriate for destriping because stripes obviously have directional characteristics. To illustrate, in Fig. 2, we show the derivatives of the regular stripes along horizontal and vertical directions of a MODIS image. It can be seen clearly that the horizontal derivative [Fig. 2(b)] contains the most stripes, while the vertical derivative [Fig. 2(c)] has very few stripes. In other words, stripes greatly vary in terms of gradient across the stripe lines, while the gradient along the stripe lines is only slightly influenced. Therefore, we attempt to constrain the gradient across the stripe lines while preserving the gradient along the stripe lines. To this end, we use the unidirectional TV to exploit the directional characteristic [15]. A similarly motivated method was proposed by researchers previously [7]. They made use of the directional characteristic via wavelet decomposition, and subsequently, they employed Fourier filters to remove the stripes in specific bands.

Thus, we formulate the unidirectional TV regularization as:

$$R_{TV}(\mathbf{u})=\|\nabla_y \mathbf{u}\|_1+\tau\|\nabla_x(\mathbf{u}-\mathbf{I}_s)\|_1, \tag{4}$$

where τ denotes the parameter that balances the constraints across and along the stripes. The parameters ∇_y and ∇_x denote the vertical and horizontal derivative operators, respectively. In this work, we regard the direction along the stripes as the x-axis and the direction across the stripes as the y-axis. The functional (4) is intuitive. The first term penalizes the ℓ_1-norm of the gradient across the stripes so as to remove the stripes while the second term enforces the ℓ_1-norm constraints on the difference between the gradient along the stripes of the desired and striped images, thereby aiming at preserving the gradient along the stripes as striped images. This approach is very reasonable since the stripes only slightly influence the gradient along the stripes. In fact, the second term of (4) is a regularity term for noise in its first order along

#196612 - $15.00 USD Received 28 Aug 2013; revised 11 Sep 2013; accepted 11 Sep 2013; published 24 Sep 2013
(C) 2013 OSA



(a) (b) (c)

Fig. 2. (a) Striped image. (b) Horizontal derivative. (c) Vertical derivative.

the x-axis, which actually is a fidelity term since it involves the difference between the restored image and the observed one. We place the two terms together to emphasize their advantage over the traditional isotropic TV in the destriping context.

In [15], the authors used a unidirectional TV model to remove the stripes. However, a weakness of their model is that it places too large a constraint on the unidirectional derivative. As a result, irregular stripes that are not strictly vertical or horizontal will not be properly handled, as observed in the case of the waterfall effect in the focused ion beam nanotomography (FIB-nt) image [Fig. 1(b)]. Besides, structural information along the same direction as the stripes will also be removed together with the stripes.

The unidirectional TV cannot properly preserve structural details, and it is unable to resolve issues such as the waterfall effect. Moreover, unidirectional TV cannot suppress random noise. In contrast, the use of the framelet can effectively address these problems. This is because large framelet coefficients occur wherever there are singularities such as edges and detail information. The framelet-based approach essentially keeps large framelet coefficients, and thus, it preserves edges and detail information [25]. In addition, framelet regularization can efficiently suppress Gaussian noise [25]. This motivates us to apply framelet regularization to destriping. Thus, we utilize the following regularization term:

$$R_{FR}(\mathbf{u}) = \left\| \mathbf{W}\mathbf{u} \right\|_1, \tag{5}$$

where $\mathbf{W}$ represents the framelet transform using the filters of the framelet system. This framelet regularization term penalizes the ℓ_1-norm of the framelet transform coefficients of the image $\mathbf{u}$. In this work, we use the B-splines framelet. Further details on the theory and implementation on the framelet transform can be found in [26, 27]. Thus, the final energy functional about $\mathbf{u}$ is:

$$\min_{\mathbf{u}} \frac{1}{2}\left\| \mathbf{u} - \mathbf{I_s} \right\|_2^2 + \lambda_1 \left\| \mathbf{W}\mathbf{u} \right\|_1 + \lambda_2 \left\| \nabla_y \mathbf{u} \right\|_1 + \lambda_3 \left\| \nabla_x (\mathbf{u} - \mathbf{I_s}) \right\|_1. \tag{6}$$

To simplify the notations used, we set the regularization parameters as $\lambda_1, \lambda_2, \lambda_3$, respectively. The difficulties in determining $\mathbf{u}$ are that the ℓ_1-norm terms are nonsmooth and nonseparable. The existing optimization methods, such as gradient descent, cannot be directly used.

2.2 Numerical algorithm

The split Bregman method [28] is an efficient tool to solve ℓ_1-norm regularizations. The split Bregman iteration technique offers several advantages over conventional optimization methods. First, the iteration avoids the problem of numerical instabilities wherein

#196612 - $15.00 USD Received 28 Aug 2013; revised 11 Sep 2013; accepted 11 Sep 2013; published 24 Sep 2013
(C) 2013 OSA

nondifferentiable points exist when using continuation methods, particularly for the ℓ_1-norm. Second, the split Bregman iteration converges quickly with less memory usage, which makes it attractive for addressing large-scale problems and for real-time applications.

The basic idea of split Bregman iteration is to convert the unconstrained minimization problem on $\mathbf{u}$ in (6) into a constrained one by introducing three auxiliary variables $\mathbf{d} = \mathbf{W}\mathbf{u}$, $\mathbf{d}_x = \nabla_x(\mathbf{u} - \mathbf{I_s})$, and $\mathbf{d}_y = \nabla_y \mathbf{u}$. The minimization (6) is equivalent to the constrained problem:

$$\min_{\mathbf{u}} \frac{1}{2}\left\|\mathbf{u} - \mathbf{I_s}\right\|_2^2 + \lambda_1 \left\|\mathbf{d}\right\|_1 + \lambda_2 \left\|\mathbf{d}_y\right\|_1 + \lambda_3 \left\|\mathbf{d}_x\right\|_1 \text{ s.t. } \mathbf{d} = \mathbf{W}\mathbf{u}, \mathbf{d}_x = \nabla_x(\mathbf{u} - \mathbf{I_s}), \mathbf{d}_y = \nabla_y \mathbf{u}. \quad (7)$$

Subsequently, by strictly enforcing the constraints by applying the Bregman iteration, the problem (7) can further be transformed into a nonconstrained minimization:

$$\begin{aligned} \min_{\mathbf{u},\mathbf{d},\mathbf{d}_x,\mathbf{d}_y} & \frac{1}{2}\left\|\mathbf{u} - \mathbf{I_s}\right\|_2^2 + \lambda_1 \left\|\mathbf{d}\right\|_1 + \lambda_2 \left\|\mathbf{d}_y\right\|_1 + \lambda_3 \left\|\mathbf{d}_x\right\|_1 \\ & + \frac{\alpha}{2}\left\|\mathbf{d} - \mathbf{W}\mathbf{u} - \mathbf{b}\right\|_2^2 + \frac{\beta}{2}\left\|\mathbf{d}_y - \nabla_y \mathbf{u} - \mathbf{b}_y\right\|_2^2 + \frac{\gamma}{2}\left\|\mathbf{d}_x - \nabla_x(\mathbf{u} - \mathbf{I_s}) - \mathbf{b}_x\right\|_2^2, \end{aligned} \quad (8)$$

where α, β, γ denote penalization parameters. This is the split Bregman iteration. Clearly, the minimizations of (8) with respect to $\mathbf{u}, \mathbf{d}, \mathbf{d}_x$, and $\mathbf{d}_y$ can be decoupled, and thus, they can be further converted into four separate subminimization problems.

• The **u**-related subproblem is given by

$$\min_{\mathbf{u}} \frac{1}{2}\left\|\mathbf{u} - \mathbf{I}_s\right\|_2^2 + \frac{\alpha}{2}\left\|\mathbf{d}^k - \mathbf{W}\mathbf{u} - \mathbf{b}^k\right\|_2^2 + \frac{\beta}{2}\left\|\mathbf{d}_y^k - \nabla_y \mathbf{u} - \mathbf{b}_y^k\right\|_2^2 + \frac{\gamma}{2}\left\|\mathbf{d}_x^k - \nabla_x(\mathbf{u} - \mathbf{I_s}) - \mathbf{b}_x^k\right\|_2^2, \quad (9)$$

which is a least-square problem. It is equivalent to the following linear system:

$$\begin{aligned} & (\alpha \mathbf{W}^T\mathbf{W} + \beta \nabla_y^T \nabla_y + \gamma \nabla_x^T \nabla_x + \mathbf{I})\mathbf{u}^{k+1} \\ & = \alpha \mathbf{W}^T(\mathbf{d}^k - \mathbf{b}^k) + \beta \nabla_y^T(\mathbf{d}_y^T - \mathbf{b}_y^T) + \gamma \nabla_x^T(\mathbf{d}_x^k + \nabla_x \mathbf{I}_s - \mathbf{b}_x^k) + \mathbf{I_s}. \end{aligned} \quad (10)$$

It is to be noted that $\mathbf{W}^T\mathbf{W} = \mathbf{I}$, and (10) can be solved by the fast Fourier transform efficiently.

• The **d**-related subproblem is

$$\min_{\mathbf{d}} \lambda_1 \left\|\mathbf{d}\right\|_1 + \frac{\alpha}{2}\left\|\mathbf{d} - \mathbf{W}\mathbf{u}^{k+1} - \mathbf{b}^k\right\|_2^2. \quad (11)$$

The subproblem in (11) can be solved by using a shrinkage operator as follows:

$$\mathbf{d}^{k+1} = shrink(\mathbf{W}\mathbf{u}^{k+1} + \mathbf{b}^k, \frac{\lambda_1}{\alpha}), \quad (12)$$

where

$$shrink(r, \xi) = \frac{r}{|r|} * \max(r - \xi, 0). \quad (13)$$

The shrink operator represents the soft thresholding method proposed in [29]. This shrinkage is extremely fast and requires only a few operations per element of **d**.

Similarly, $\mathbf{d}_y$ and $\mathbf{d}_x$ can be obtained as $\mathbf{d}$ parallelly. Thus, $\mathbf{d}$, $\mathbf{d}_y$ and $\mathbf{d}_x$ can be expressed as:

#196612 - $15.00 USD Received 28 Aug 2013; revised 11 Sep 2013; accepted 11 Sep 2013; published 24 Sep 2013
(C) 2013 OSA

$$\begin{cases} \mathbf{d}^{k+1} = shrink(\mathbf{W}\mathbf{u}^{k+1} + \mathbf{b}^{k}, \dfrac{\lambda_1}{\alpha}), \\ \mathbf{d}_y^{k+1} = shrink(\nabla_y \mathbf{u}^{k+1} + \mathbf{b}_y^{k}, \dfrac{\lambda_2}{\beta}), \\ \mathbf{d}_x^{k+1} = shrink(\nabla_x (\mathbf{u}^{k+1} - \mathbf{I}_s) + \mathbf{b}_x^{k}, \dfrac{\lambda_3}{\gamma}). \end{cases} \tag{14}$$

Finally, we update the Bregman variables $\mathbf{b}^{k+1}, \mathbf{b}_y^{k+1}$ and $\mathbf{b}_x^{k+1}$ in the following manner:

$$\begin{cases} \mathbf{b}^{k+1} = \mathbf{b}^{k} + (\mathbf{W}\mathbf{u}^{k+1} - \mathbf{d}^{k+1}), \\ \mathbf{b}_y^{k+1} = \mathbf{b}_y^{k} + (\nabla_y \mathbf{u}^{k+1} - \mathbf{d}_y^{k+1}), \\ \mathbf{b}_x^{k+1} = \mathbf{b}_x^{k} + (\nabla_x (\mathbf{u}^{k+1} - \mathbf{I}_s) - \mathbf{d}_x^{k+1}). \end{cases} \tag{15}$$

Taking into account the above equations, we obtain the complete iteration used in our algorithm for destriping (see the section entitled Algorithm for a detail description).

Algorithm Image destriping with sparsity regularizations

Input $\mathbf{u}_0 = \mathbf{I_s}$ {Initialize $\mathbf{u}_0$ with the observed image I_s }

While ($\left\|\mathbf{u}^{k+1} - \mathbf{u}^{k}\right\| / \left\|\mathbf{u}^{k+1}\right\| > \varepsilon$ *and* $k < N_{\max}$) **do**

Update $\mathbf{u}^{k+1}$ by (10)

Solve (14) for $\mathbf{d}^{k+1}, \mathbf{d}_y^{k+1}, \mathbf{d}_x^{k+1}$

Update $\mathbf{b}^{k+1}, \mathbf{b}_y^{k+1}$ and $\mathbf{b}_x^{k+1}$ by(15)

end While

Output: Destriping image = $\mathbf{u}^{k+1}$

3. Experiments and discussion

In simulated experiments, an original 256 × 256 Lena image was used. The striped images were simulated by adding stripe lines to the original image. All the test images were normalized to [0, 1]. We compared the proposed algorithm with wavelet-Fourier combining filtering used in [7] (wavelet-FFT), the Huber regularization model used in [12] (Huber-Reg), the unidirectional TV algorithm used in [15] (Uni-TV), and the variational stationary noise remover algorithm used in [14] (VSNR). The wavelet-FFT algorithm implementation was kindly provided by Dr. Beat Münch [7].

In actual experiments, in order to test the proposed algorithm for different stripes, we selected four kinds of stripe images: a FIB-nt image, an AFM image, a PMMW image, and a MODIS image. Further, the actual images were normalized to [0, 1].

Certain qualitative and quantitative assessments were performed to provide an overall evaluation. The qualitative assessments included visual destriping performance and the calculation and comparison of the mean cross-track profile. The peak signal-to-noise ratio (PSNR) was used to measure the destriping quality for the simulated images.

$$PSNR = 10\log_{10}\left(\frac{N}{\left\|\mathbf{u} - \mathbf{I}_s\right\|^2}\right), \tag{16}$$

where N denotes the total number of image pixels. Moreover, the non-referenced image quality Q-metric is used to evaluate the denoising performance [30]. For the two indices, the higher the value is, the better is the image quality.

#196612 - $15.00 USD Received 28 Aug 2013; revised 11 Sep 2013; accepted 11 Sep 2013; published 24 Sep 2013
(C) 2013 OSA



Fig. 3. Simulated experiment with image containing severe stripes. (a) Original image. (b) Simulated striped image with severe additive stripes. Destriping results obtained using (c) wavelet-FFT, (d) Uni-TV, (e) proposed model without framelet regularization (FR) term, and (f) proposed algorithm.

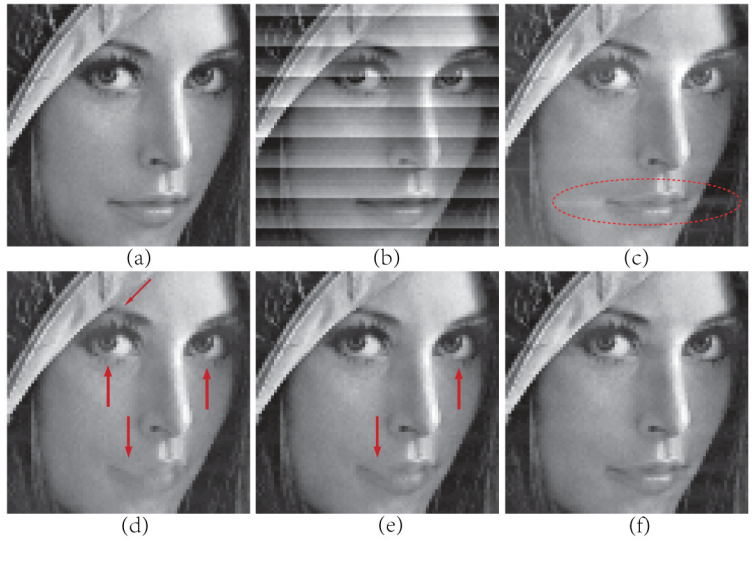


Fig. 4. Detail regions cropped from Fig. 3.

Table 1. PSNR (dB) values for Lena image with severe stripes.

Index	Wavelet-FFT	Uni-TV	Without FR	Proposed
PSNR	24.97	30.49	33.02	**33.31**

#196612 - $15.00 USD Received 28 Aug 2013; revised 11 Sep 2013; accepted 11 Sep 2013; published 24 Sep 2013
(C) 2013 OSA

3.1 Simulation experiments

Figure 3(a) shows the original selected image. The striped image, shown in Fig. 3(b), was obtained by adding eight successive stripe lines per ten lines. The magnitude of the stripes ranges from –40 to 40. From Fig. 3(c), it can be observed that the application of the wavelet-FFT algorithm decreases the contrast. Figure 3(d) shows the destriping result obtained using Uni-TV, wherein certain features lying along the same direction as the stripes are degraded along with the stripes, such as the mouth and the shoulder. This is because the unidirectional TV approach lays emphasis on the smoothness of the images along a certain direction such that it tends to yield excessively destriped results. A similar phenomenon is also observed in Fig. 3(e), which is acquired by the proposed model without using the framelet regularization term. Obviously, a satisfactory result is achieved in Fig. 3(f) by the proposed algorithm. The stripes are effectively removed because of the presence of Uni-TV terms and the structural details are satisfactorily preserved due to the framelet regularization term.

For convenience of comparison, the detail regions cropped from Fig. 3 are displayed in Fig. 4, wherein the images show abundant structural details. The wavelet-FFT method obviously decreases the contrast, as shown in Fig. 4(c). In Figs. 4(d)-4(e), it can be seen that the mouth and the eyelashes are badly corrupted. With the proposed algorithm, Fig. 4(f), the stripes are fully removed and the detail information is well-preserved.

To demonstrate the method's effectiveness in suppressing random noise, we performed a second simulated experiment. Figure 5(a) shows the striped image with additional Gaussian noise ($\sigma = 8$). The magnitudes of the stripe noise range from –40 to 40. These noise magnitudes are consistent with those that realistically occur in actual imaging systems such as the MODIS imaging system. We observe that the proposed method gives better restoration results when compared with those of other methods. In Fig. 5(i), not only are the stripes removed effectively but also random noise is well-suppressed. However, in Figs. 5(b)-5(e), we observe that the stripes have been removed while the Gaussian random noise still exists. That is, the abovementioned destriping methods are not able to satisfactorily suppress random noise in the destriping process. Figures 5(f)-5(h) show the results of wavelet shrinkage (WS) denoising [31] applied to the destriping results shown in Figs. 5(c)-5(e). It can be observed that the results obtained by the combined method (destriping + WS denoising) are not as smooth as those obtained with the proposed method. It is to be noted that the destriping result in Fig. 5(e) is achieved by the proposed model without the use of the framelet regularization term. Comparing Fig. 5(e) with Fig. 5(i), we can conclude that framelet regularization suppresses random noise substantially.

The quantitative assessments are listed in Tables 1 and 2. Every result reported is an average over 5 trails for different realizations of noise. The mean and standard deviation of the PSNR value are denoted by M-PSNR and S-PSNR, and those of the Q-metric are denoted by M-Q-metric and S-Q-metric. It can be seen that the proposed algorithm consistently provides the best PSNR and Q-metric values for different levels of stripes and Gaussian noise. The simulated experiment results show that the proposed method significantly enhances the stripe-removal performance and random noise as well as perfectly preserving the structural details.

3.2 Actual experiments

3.2.1 Elimination of the waterfall effect in focused ion beam nanotomography imaging

FIB-nt is a three-dimensional imaging technique with nanometric resolution, which uses dual (electron and ion) beam microscopy [32]. FIB-nt imaging often results in irregular stripes caused by the occurrence of material phases in the sample microstructure, namely the waterfall effects [33, 34], as shown in Fig. 6(a). This image was obtained from a previous study [7]. As mentioned in [7], waterfall effects are particularly challenging problems, since the stripes are not strictly horizontal or vertical. In addition, the stripes in FIB-nt images are distributed randomly.

#196612 - $15.00 USD Received 28 Aug 2013; revised 11 Sep 2013; accepted 11 Sep 2013; published 24 Sep 2013
(C) 2013 OSA



Fig. 5. Simulated experiment using image with random noise. (a) Striped image with Gaussian noise. Destriping results obtained using (b) wavelet-FFT, (c) Uni-TV, (d) VSNR, (e) proposed model without framelet regularization (FR) term, (f) Uni-TV + wavelet shrinkage (WS), (g) VSNR + WS, (h) proposed model without framelet regularization (FR) term + WS, and (i) complete proposed method.

Table 2. PSNR (dB) and Q-metric values for Lena image with stripes and random noise.

Index	Wavelet-FFT	Uni-TV	VSNR	Without FR	Uni-TV + WS	VSNR + WS	Without FR + WS	Proposed
M-PSNR	27.48	27.84	32.90	32.32	28.20	33.57	32.94	**34.22**
S-PSNR	0.16	0.10	0.02	0.04	0.09	**0.02**	0.04	0.03
M-Q-metric	28.37	28.15	28.34	28.41	33.65	33.87	33.83	**35.64**
S-Q-metric	0.31	0.35	0.29	0.30	0.20	0.15	0.17	**0.14**

In Fig. 6(b), wherein the image was obtained by wavelet-FFT, although most of the stripes are eliminated, some residual stripes still exist. Moreover, the image contrast is decreased, which weakens the visual quality of the destriping image. In Fig. 6(c), although

#196612 - $15.00 USD Received 28 Aug 2013; revised 11 Sep 2013; accepted 11 Sep 2013; published 24 Sep 2013
(C) 2013 OSA

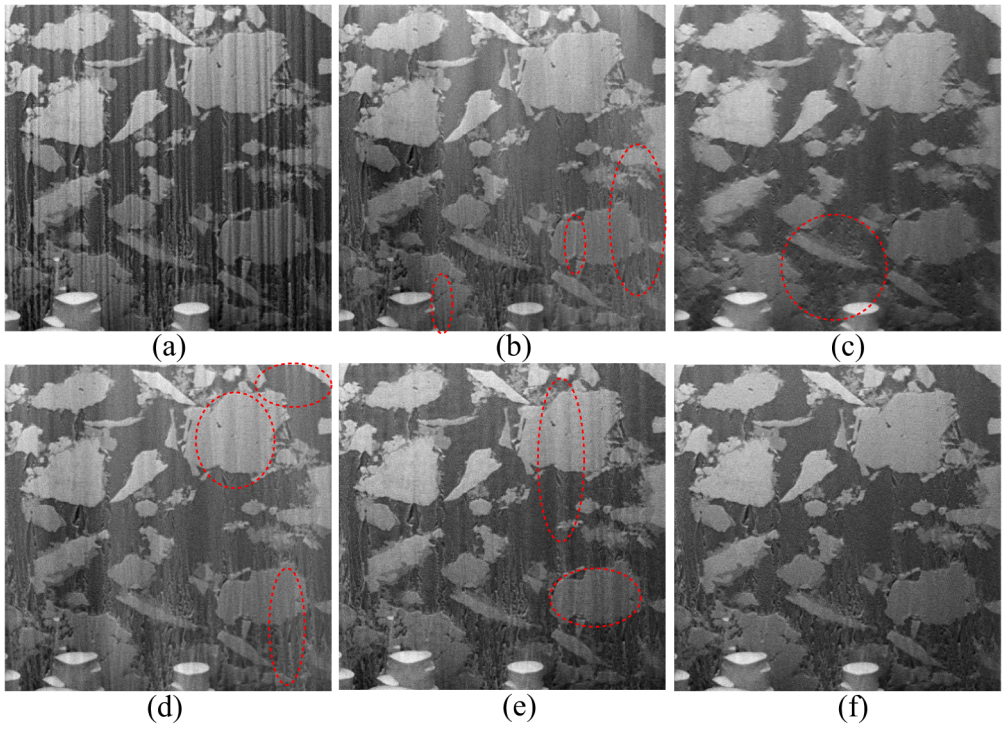


Fig. 6. (a) Original FIB-nt striped image. Destriping results obtained using (b) wavelet-FFT, (c) Huber-Reg, (d) Uni-TV, (e) VSNR, and (f) proposed algorithm.

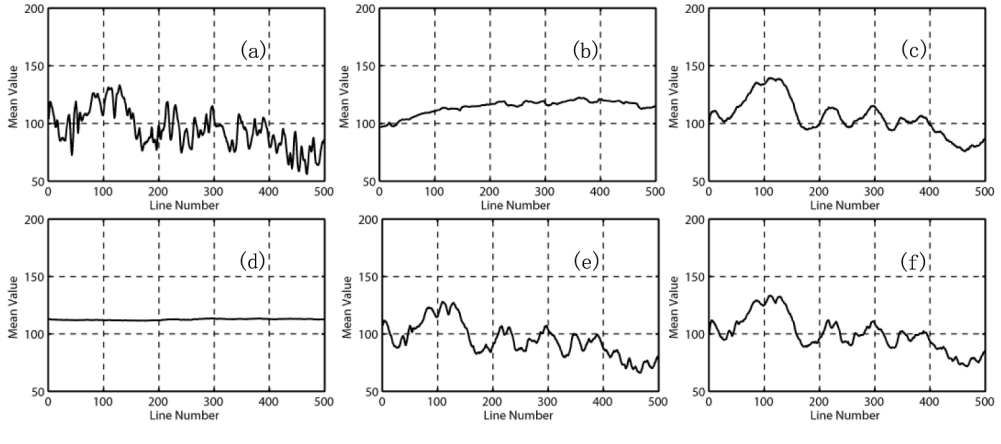


Fig. 7. Mean cross-track profiles for images shown in Fig. 6.

the stripes are completely removed, the detail information is severely degraded along with the removal of the stripes. From Fig. 6(d), we observe that the Uni-TV model can completely remove the exactly vertical stripes, but the waterfall effects still exist in the flat regions. This is because the Uni-TV model can only eliminate the stripes that are exactly horizontal or vertical. Figure 6(e) shows an image obtained via the VSNR method, which removes most of the waterfall effects, but some residual stripes can be observed in the flat regions. Obviously, the proposed method provides the best result with satisfactory visual quality. The framelet coefficients of the irregular stripes are effectively penalized by framelet regularization.

#196612 - $15.00 USD Received 28 Aug 2013; revised 11 Sep 2013; accepted 11 Sep 2013; published 24 Sep 2013
(C) 2013 OSA

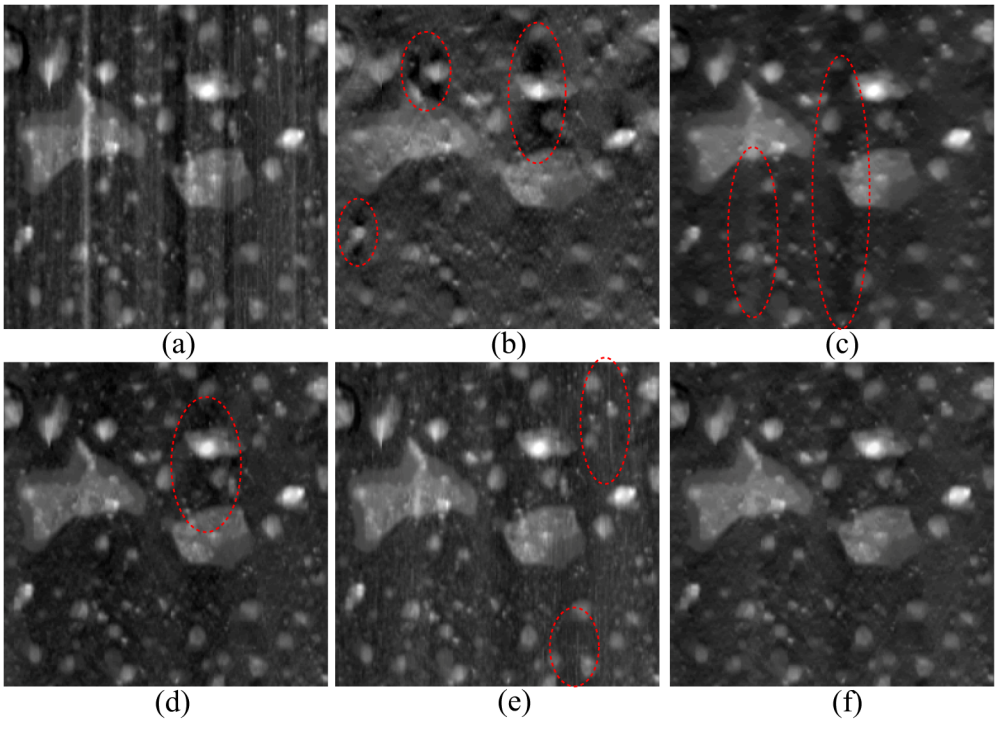


Fig. 8. (a) Original AFM striped image. Destriping results obtained using (b) wavelet-FFT, (c) Huber-Reg, (d) Uni-TV, (e) VSNR, and (f) proposed algorithm.

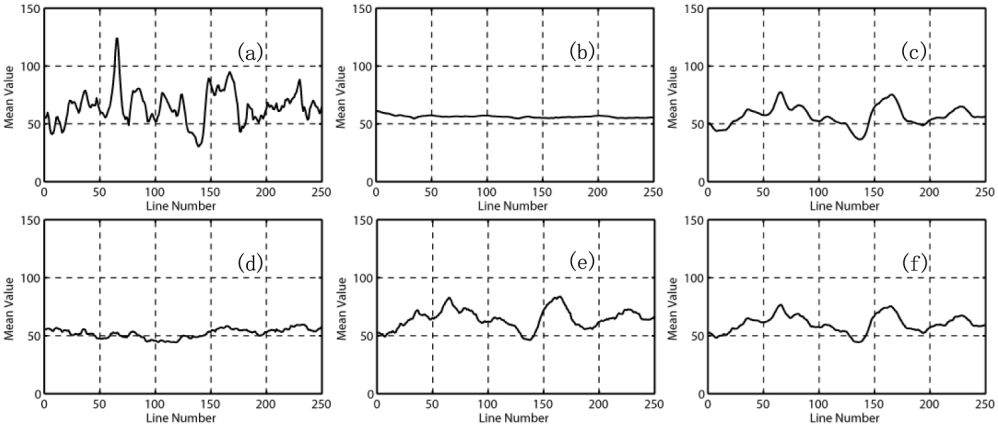


Fig. 9. Mean cross-track profiles for images shown in Fig. 8.

Consequently, irregular stripes are removed effectively. The stripes are perfectly removed without causing any noticeable artifacts, and the structural information belonging to the original FIB-nt image is well-preserved. This result shows that the proposed method is perfectly capable of removing irregular stripes while simultaneously preserving the structural detail.

Figure 7 shows the mean cross-track profiles before and after destriping. The horizontal axis represents the column number, and the vertical axis represents the mean value of each column. The mean cross-track profile of the striped image fluctuates wildly because of the stripes, while that of the healthy image exhibits a somewhat smoother curve. From Fig. 7(b),

#196612 - $15.00 USD Received 28 Aug 2013; revised 11 Sep 2013; accepted 11 Sep 2013; published 24 Sep 2013
(C) 2013 OSA

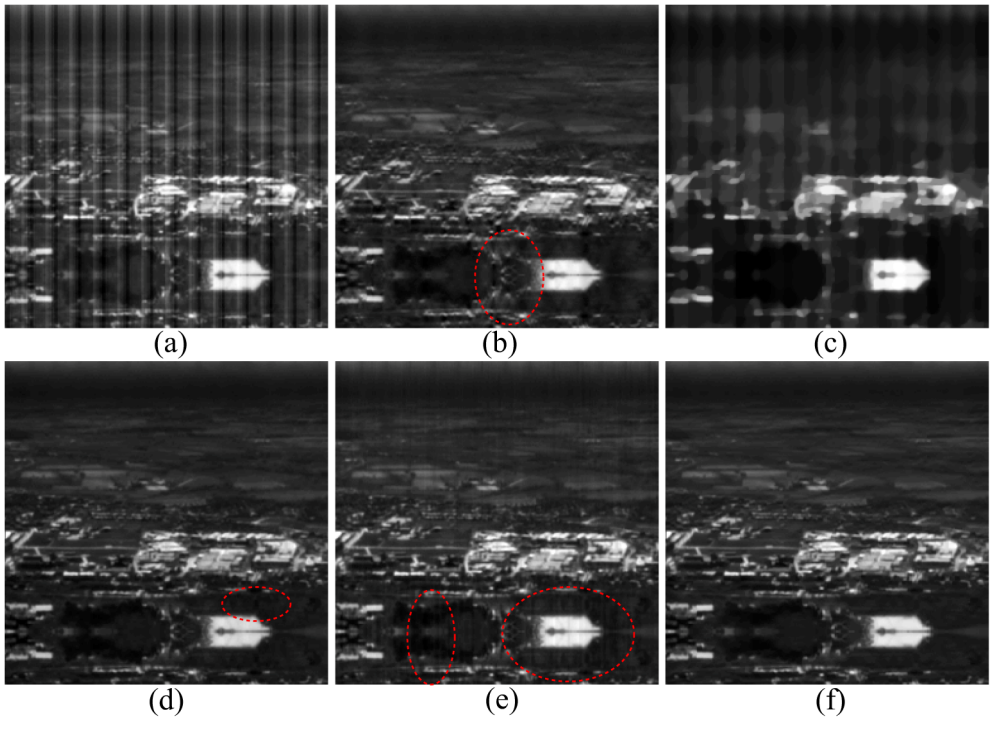


Fig. 10. (a) Original PMMW striped image. Destriping results obtained using (b) wavelet-FFT, (c) Huber-Reg, (d) Uni-TV, (e) VSNR, and (f) proposed algorithm.

we note that the mean cross-track profile is fairy different from the original, which indicates a decrease in the image contrast. In Fig. 7(d), the mean cross-track profile is excessively smoothed to nearly a straight line. Such a result is not surprising as the Uni-TV model imposes excessive smoothness along one direction on the image. Figures 7(c), 7(e) and 7(f) all show satisfactory levels of smoothness. However, the image corresponding to Fig. 7(c) is excessively smoothed, and a considerable amount of detail information is lost, while Fig. 7(e) shows a few burrs, thereby indicating the presence of a few residual stripes. Figure 7(f) shows that the proposed method can achieve an acceptable tradeoff between stripe removal and detail preservation. This is primarily because the framelet essentially preserves various types of edges while unidirectional TV aspect of the method efficiently removes the stripes.

3.2.2 Removal of non-uniform stripes and random noise in atomic force microscope

AFM imaging belongs to the family of scanning probe microscopy (SPM) techniques [1]. Because of the great binding strength between the sample and the cantilever tip, stripes are generated by the protrusive disturbances, and they severely interfere with the tip vibrational modes. As illustrated in [1], these stripes vary in formation particularly in the areas wherein sample particles are densely packed. The stripes in AFM images vary with intensity, length, density, and frequency range, all of which exhibit non-uniform characteristics. It is worth noting that the AFM image in Fig. 8(a), which was used in [1], also contains a slight amount of random noise.

In Fig. 8(b), the image that is subject to the wavelet-FFT method is free from the stripes, but it leads to loss of information, as indicated by the red mark. The Huber-Reg method applied to the image in Fig. 8(c) removes most of the stripes; however, the strong stripe artifacts can still be observed. Moreover, the detail information is unexpectedly degraded. From Fig. 8(d), it can be observed that the stripes are removed, but random noise still exists.

#196612 - $15.00 USD Received 28 Aug 2013; revised 11 Sep 2013; accepted 11 Sep 2013; published 24 Sep 2013
(C) 2013 OSA

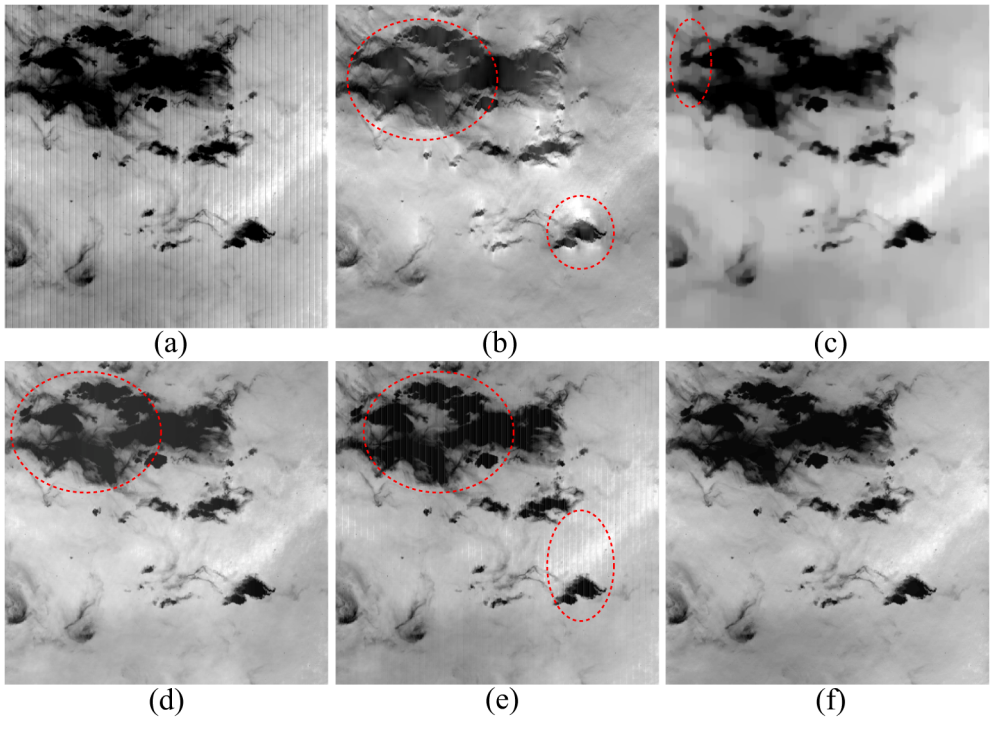


Fig. 11. (a) Original MODIS striped image. Destriping results obtained using (b) wavelet-FFT, (c) Huber-Reg, (d) Uni-TV, (e) VSNR, and (f) proposed algorithm.

In Fig. 8(e), it is obvious that the destriping result obtained via the VSNR method exhibits random stripes. In Fig. 8(f), which image is the result of applied the proposed method, a more visually satisfactory result is achieved. The stripes are perfectly removed without causing any artifacts, and the structural information belonging to the original AFM is well-preserved. Furthermore, it can be observed that the proposed method is more effective in suppressing random noise. Figure 9 reflects the results observed in Fig. 8 in terms of the mean-track cross profiles of the destriping images.

3.2.3 Removal of periodic and severe stripes in passive millimeter-wave images

Passive millimeter-waves (PMMW) are less affected by adverse weather conditions such as cloud, smoke, fog, and dust [2]. However, PMMW images suffer from poor spatial resolution because of the long wavelength of millimeter waves. Further, the existing periodic and severe stripes deteriorate the imaging quality because of the non-uniform response of the receivers of the multidetector imaging system. The PMMW image used in this study was obtained from DERA Malvern [3].

In Fig. 10(b), wherein the image has been cleaned up using the wavelet-FFT method, most stripes are removed, but certain obvious residual stripes still exist and the information loss is severe. The Huber-Reg model does not work in eliminating very severe stripes, as observed from Fig. 10(c). The Uni-TV method removes the most noticeable stripes [Fig. 10(d)], while in Fig. 10(e), some residual stripes can be observed. The proposed method [Fig. 10(f)] provides a more visually pleasing result. The severe stripes are perfectly removed without causing noticeable artifacts, and the structural information is well-preserved. In addition, it is worth noting that the regions corrupted by the severe stripes have been well “inpainted” by the proposed method.

#196612 - $15.00 USD Received 28 Aug 2013; revised 11 Sep 2013; accepted 11 Sep 2013; published 24 Sep 2013
(C) 2013 OSA

3.2.4 Removal of incomplete stripes in moderate resolution imaging spectroradiometer

The MODIS imaging technique uses 36 spectral bands ranging from the visible (0.4 μm) to the long-wave-infrared (14.4 μm). MODIS has been used extensively in land, ocean, and atmospheric imaging; consequently, this has led to some remarkable advances in the earth sciences. We chose Terra MODIS level 1 B data for our study, which were downloaded from http://ladsweb.nascom.nasa.gov/. As shown in Fig. 11(a), some of the stripes in this image band 27 are incomplete, for instance in the dark regions of the image.

In Fig. 11(b), the stripes are almost completely removed by the wavelet-FFT method, but the result exhibits information loss. In Fig. 11(c), obvious piecewise constant artifacts are observed. From Fig. 11(d), it can be observed that the stripes have been removed, while the information in the dark regions is unexpectedly degraded. With the VSNR method [Fig. 11(e)], residual stripes in the bright regions can be seen. Although the stripes are mostly removed, some extra stripes are introduced in the dark regions. In Fig. 11(f), the stripes are perfectly removed without the introduction of noticeable artifacts.

Overall, the results of the proposed method are consistent for all test images, and they exhibit good visually quality with fewer artifacts than the results obtained with the other methods. The stripes and random noise are significantly suppressed and the detail information is perfectly preserved by the proposed method, while the existing destriping methods more or less exhibit their limitations in handling different stripes.

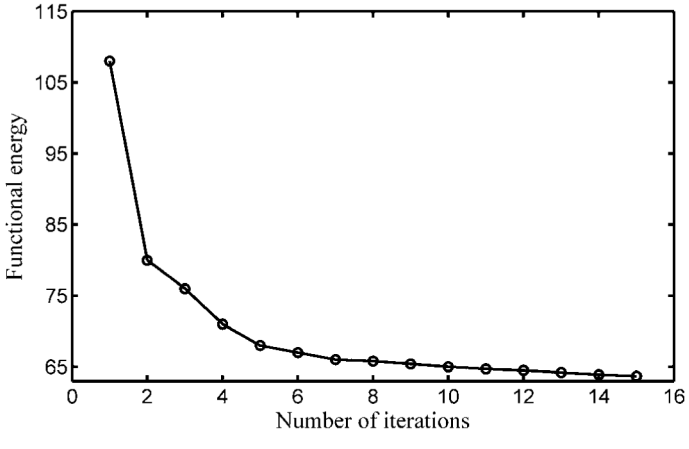


Fig. 12. Evolution of functional energy versus number of iterations for the proposed method.

3.3 Convergence rate of the algorithm and parameter determination

We investigated the convergence behavior of the proposed algorithm in the next phase of the study. Figure 12 illustrates the evolutional curve of the functional energy versus the iterations for the PMMW test, whose imaging results are shown in Fig. 10. It can be seen clearly that the proposed method achieves good convergence and converges after about 10 iterations.

Moreover, in order to validate the robustness of the proposed method for the selection of regularization parameters, we performed a sensitivity analysis for the three regularization parameters for different stripe noise levels. Figure 13 shows the curve of PSNR values versus the different regularization parameters. In case 1, weak stripe noise (four stripe lines per ten lines) is added into the Lena image [Fig. 13(a)]. In case 2, severe stripe noise (eight stripe lines per ten lines) is added into the Lena image [Fig. 13(b)]. In Figs. 13(d)-13(e), it is clearly shown that the destriping results exhibit robustness despite variations in the parameters λ_2 and λ_3. We carried our testing using different noise levels for the parameter λ_1, and we empirically

#196612 - $15.00 USD Received 28 Aug 2013; revised 11 Sep 2013; accepted 11 Sep 2013; published 24 Sep 2013
(C) 2013 OSA

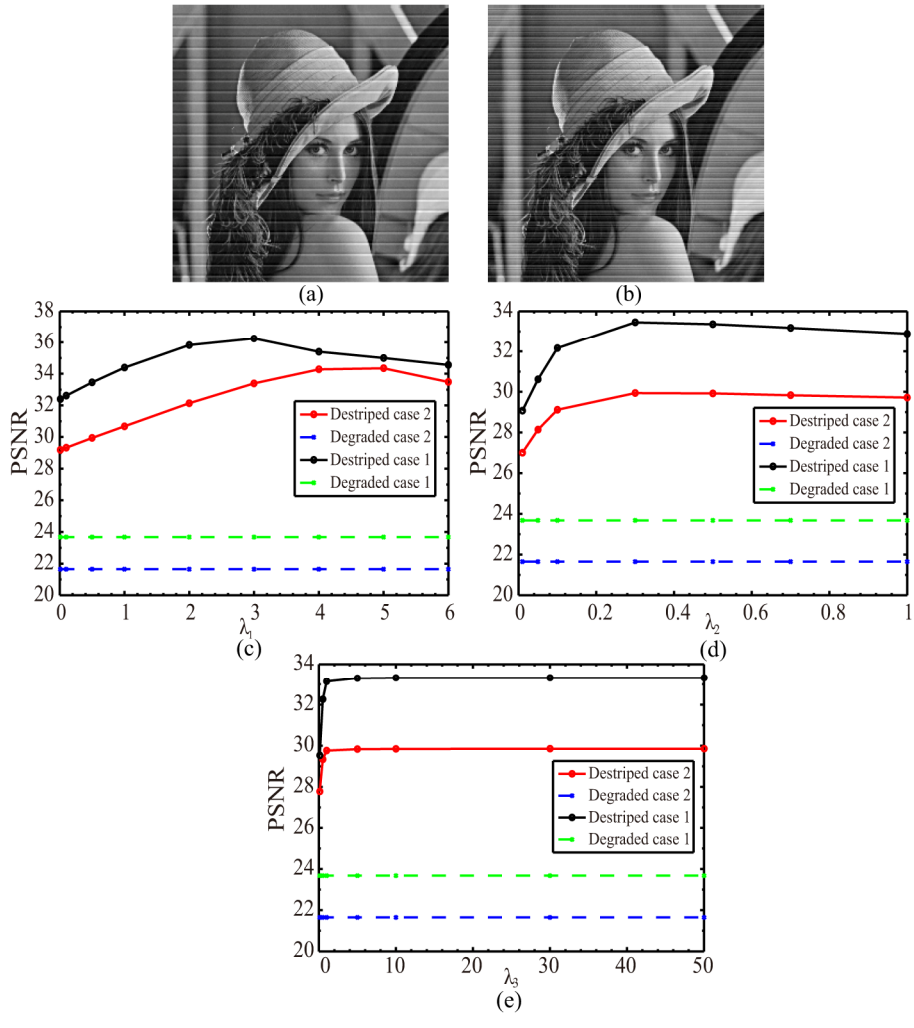


Fig. 13. (a) Image with weak stripe noise. (b) Image with severe stripe noise. (c)-(e) Curve of PSNR values versus parameters λ_1, λ_2, and λ_3, respectively.

determined that the best PSNR values are achieved when $\lambda_1 \in [3, 5]$, as shown in Fig. 13(c). There exists a global maximum in each PSNR curve when the parameter λ_1 lies between 3 and 5. Experimental results for other images show that these parameter ranges are universal.

In our implementation, we empirically set the parameter ranging as $\lambda_1 \in [3, 5]$, $\lambda_2 \in [0.1, 1]$, and $\lambda_3 \in [5, 10]$, and the corresponding Bregman parameter was set as $\alpha \in [10, 1000]$, $\beta \in [10, 50]$, and $\gamma \in [50, 100]$. Parameter λ_2 depends on the degree of the image stripe. Images with severe stripes require a larger value of λ_2. Images with Gaussian noise require a larger value λ_1.

3.4. Limitation

The aforementioned experiments indicate that the proposed algorithm is effective for removing additive stripes. However, for stripes which are mainly caused by the multiplicative component, the proposed additive model cannot be used. An alternative is to obtain the logarithm of the image before performing the destriping process to make the noise additive [13]. In addition, for FIB-nt and AFM images, there is not any physical model of the stripes, meaning that a more reasonable model can be proposed. This issue is an open problem.

#196612 - $15.00 USD Received 28 Aug 2013; revised 11 Sep 2013; accepted 11 Sep 2013; published 24 Sep 2013
(C) 2013 OSA

4. Conclusion

In this study, we proposed and implemented a new destriping method combining unidirectional total variation and framelet regularization. The method shows satisfactory robustness by exploiting the sparsity of the images in both the gradient and framelet domains, and it can completely remove different kinds of stripes while simultaneously satisfactorily preserving the structural details of the image. Not only could the regular stripes be completely removed by the proposed method, but the irregular stripes were also completely removed. Moreover, our method is also capable of suppressing random noise in imaging systems as opposed to many of the currently existing destriping techniques. The split Bregman iteration algorithm is introduced to solve the resulting minimization problem in order to reduce the normally large computation load. Once $\mathbf{u}^{k+1}$ is obtained via (10), the three equations given by (14) can be computed parallelly. Subsequently, the three equations given by (15) can be also calculated parallelly, and this ease of the calculation makes the proposed method more preferable for practical application. The qualitative and quantitative assessment results demonstrate that the proposed method consistently outperforms the other methods for all test images.

Although the parameter setting in our work is simple and does not involve rigorous tuning, it is preferable for use in certain applications wherein it is required to have a completely automatic parameter setting process. In future, we plan to incorporate optimal-parameter-setting methods such as the generalized cross-validation techniques [35] into our method.

Acknowledgment

The authors would like to thank Dr. Beat Münch and Dr. Pierre Weiss for helpful discussions. This work is supported by the Fundamental Research Funds for the Central Universities, HUST: 2013TS131 and National Natural Science Foundation of China under Grant 60902060. The authors would also like to thank the handling editor and anonymous reviewers for their valuable suggestions.

#196612 - $15.00 USD Received 28 Aug 2013; revised 11 Sep 2013; accepted 11 Sep 2013; published 24 Sep 2013
(C) 2013 OSA